Supplementary Material to:

X-ray absorption spectroscopy study of Mn reference compounds for Mn speciation in terrestrial surface environments

TERESA ZAHORANSKY[a], ANNA V. WEGORZEWSKI[b], WINNIE HUONG[a], CHRISTIAN MIKUTTA[a]

[a]Soil Mineralogy, Institute of Mineralogy, Gottfried Wilhelm Leibniz University Hannover, Callinstr. 3, D-30167 Hannover, Germany

[b]Federal Institute for Geosciences and Natural Resources (BGR), Stilleweg 2, D-30655 Hannover, Germany

Contents:

1. Synthesis of Mn(II) adsorption samples

Batch Mn(II) adsorption experiments were performed with a natural 85:15-90:10 illite-smectite mineral from Füzérradvány, Hungary (<2-µm fraction; Dohrmann et al., 2009) and peat from a raised peat bog (Federseemoor) near Bad Buchau, Germany (40-250-µm fraction; Hoffmann et al., 2012). Both adsorbents were previously homogenized with agate mortar and pestle. Stock solutions of Mn(II) (10 mM) were prepared from $MnCl_2$ (98%, Merck) or $MnCl_2{\cdot}4H_2O$ (p.a., Roth) and ultrapure water (>18.2 MΩ·cm), which was purged with N_2 for a minimum of two hours to remove CO_2 and O_2. After Mn(II) addition, the suspension pH was adjusted to 5 or 7 with HNO_3 or NaOH. The suspensions (2 g/L solid concentration) were horizontally shaken (100 rpm) in the dark at room temperature for 24 hours, centrifuged, and vacuum-filtered through 12-25-µm cellulose filter papers (Whatman). The filter residues were rinsed with ultrapure water, shock-frozen in liquid N_2, freeze-dried, and stored in the dark at room temperature. Adsorbed Mn was calculated as the difference between initial Mn concentrations and Mn concentrations determined in the filtrates using inductively coupled plasma–mass spectrometry (Agilent 8900). Results are reported in Table 1.

2. X-ray diffraction patterns of Mn reference compounds

Diffractograms of Mn reference compounds are shown in Figures S1 and S2. Mineral identities were confirmed in all cases using literature data and reference patterns (Table S1). Here, we only detail important features of the diffractograms (e.g., impurities).

Phyllo- and tectomanganates. Acid Na-birnessite showed four broad diffraction peaks. The peaks located at 11.7 and 24.0° 2theta were also visible for triclinic Na-birnessite and arise from (001) and (002) reflections of stacked octahedral sheets (Villalobos et al., 2003). Compared to triclinic Na-birnessite, both peaks were slightly shifted by about -0.4°. The broad peaks at 36.8 and 66.0° 2theta correspond to d-values of 2.4 and 1.4 Å respectively. The resulting d-value quotient of 1.71 is close to the expected ratio of unit-cell parameters, *b/a,* for hexagonal symmetry (Villalobos et al., 2003). δ-MnO_2 was characterized by broad *hkl* diffraction bands caused by its X-ray amorphous character. The poorly resolved basal (001) peak and the absence of a (002) reflection are typical features of δ-MnO_2 (Chukhrov et al., 1987; Chukhrov and Gorshkov, 1980; Post, 1999), indicating a small number of randomly stacked sheets per diffracting particle (Chukhrov et al., 1987; Grangeon et al., 2008). As with acid Na-birnessite, a hexagonal layer symmetry was evident from the broad peaks at ~37.4 and ~65.8° 2theta, corresponding to a d-value quotient of 1.71.

Triclinic Na-birnessite showed a set of sharp and well-defined reflections, indicating a high crystallinity. The peak at 19.3° 2theta could not be assigned to any phase. Hausmannite, a typical interstitial phase that can form during synthesis, could be excluded.

The XRD patterns of natural and synthetic cryptomelanes showed a perfect match of all reflections. Compared to the natural mineral, the reflections of synthetic cryptomelane had smaller widths, suggesting a slightly higher crystallinity. Synthetic cryptomelane showed one additional sharp peak at 8.7° 2theta, which could not be explained. Remains of the acid birnessite precursor phase were not detectable.

Natural and synthetic pyrolusites exhibited similar XRD patterns with the main (110) reflection at 28.6° 2theta. Natural pyrolusite showed two small additional peaks at 26.2°and 34.0° 2theta caused by a manganite impurity. The sharper reflections of synthetic as compared to natural pyrolusite indicate a higher crystallinity of the synthetic mineral.

Ramsdellite showed main (110) and (130) reflections at 21.8 and 35.1° 2theta. The XRD pattern was characterized by sharp diffraction peaks, indicating a high degree of crystallinity. Pyrolusite was identified as an impurity phase.

The diffractogram of synthetic Ba-free romanèchite was similar to that presented in Shen et al. (2005) with characteristic (200) and (400) reflections at 12.5 and 25.1° 2theta. However, the typically small (001) reflection at ~9.2° 2theta (d ~9.7 Å) was not observed, potentially caused by preferred orientation of the needle-shaped crystals along [001]. The peak labelled as (-311) in Shen et al. (2004) actually lies at ~38.0° 2theta (Turner and Post, 1988).

Oxide minerals without layer or tunnel structure. Natural and synthetic bixbyites showed nearly identical XRD patterns, which are in agreement with the standard pattern of bixbyite. Synthetic bixbyite had an additional peak at 28.8° 2theta, likely from a pyrolusite impurity.

Mn(III) oxyhydroxides. The peaks at 29.5 and 43.2° 2theta in the diffraction pattern of groutite originated from calcite. Additional reflections of a manganite impurity appeared at 26.4, 33.7, 37.1, 54.4, and 55.6° 2theta. All other peaks were consistent with groutite.

Carbonate, phosphate, and silicate minerals. The XRD pattern of braunite was fully consistent with the corresponding reference pattern. Additional reflections originated from quartz.

The XRD pattern of hendricksite showed additional small peaks of another mica, likely annite, the Fe-endmember of trioctahedral micas. Diffraction patterns of hendricksite and masutomilite were influenced by preferred orientation, resulting in enhanced 00*l* reflections. However, peak displacements due to preferred orientation (da Silva and de Oliveira, 2011) were not observed.

The XRD pattern of triplite was consistent with a solid-solution of triplite and zwiselite, the Fe-endmember of this mineral group. As evidenced by EPMA, the sample contained a considerable amount of Fe^{2+} (0.74 apfu; Tables 1 and S2). The diffraction pattern was intermediate between triplite and zwiselite and therefore showed occasional double peaks.

Compounds used for Mn(II) adsorption. The 'illite' sample was a natural 85:15-90:10 R3-ordered illite-smectite mixed layer mineral (Dohrmann et al., 2009). Its diffraction pattern showed prominent 00*l* reflections at 8.6, 17.8, 26.6 and 45.3° 2theta, which are common to illite and smectite minerals. Contributions of other crystalline mineral phases were not detected. The peat material was characterized by broad diffuse scattering and a single quartz reflection at 26.6° 2theta.

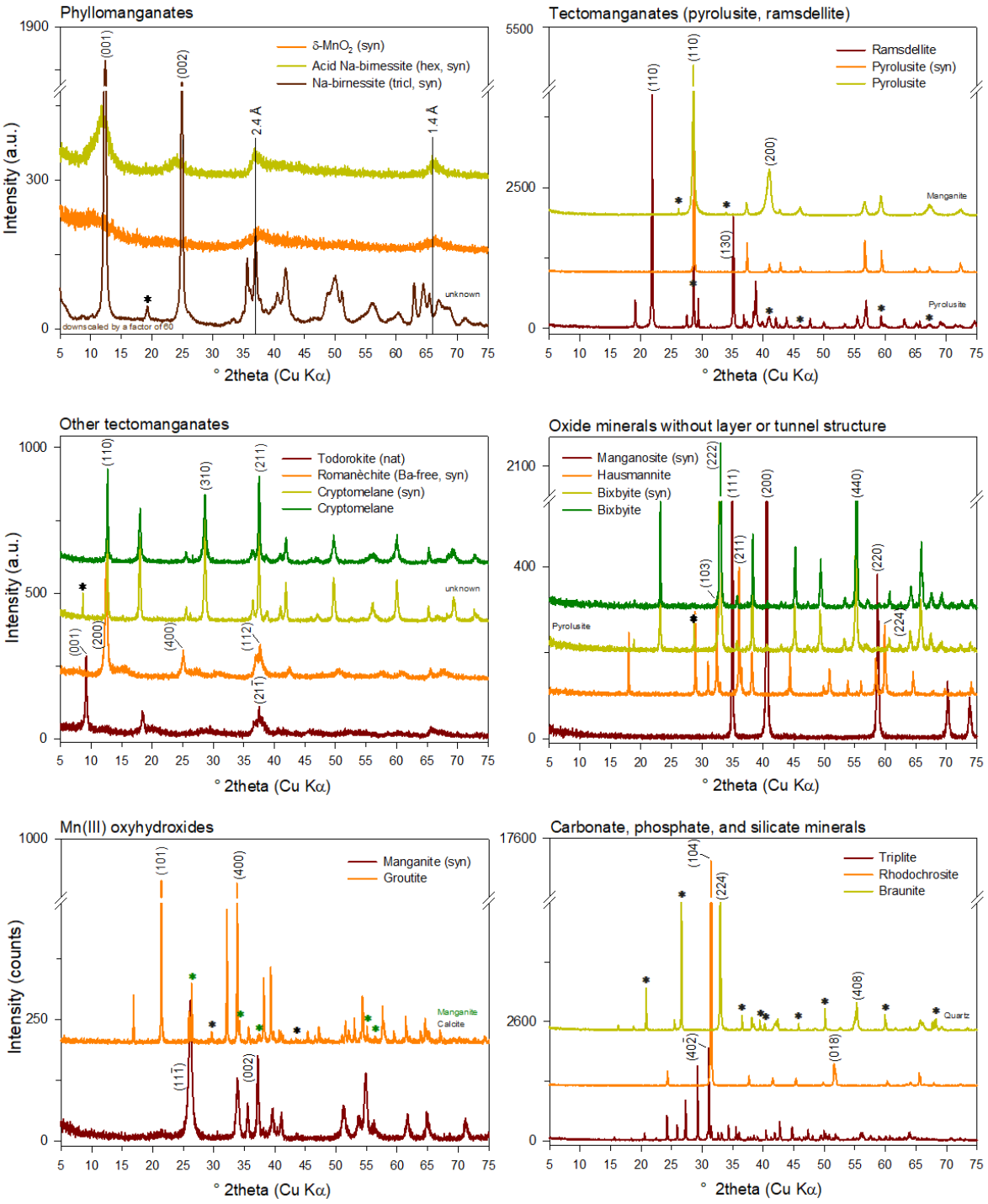

Figure S1. Diffractograms of phyllo- and tectomanganates, oxide minerals without layer or tunnel structure, Mn(III) oxyhydroxides as well as carbonate, phosphate, and silicate minerals. Main reflections are indexed and asterisks indicate impurities (see text for further details).

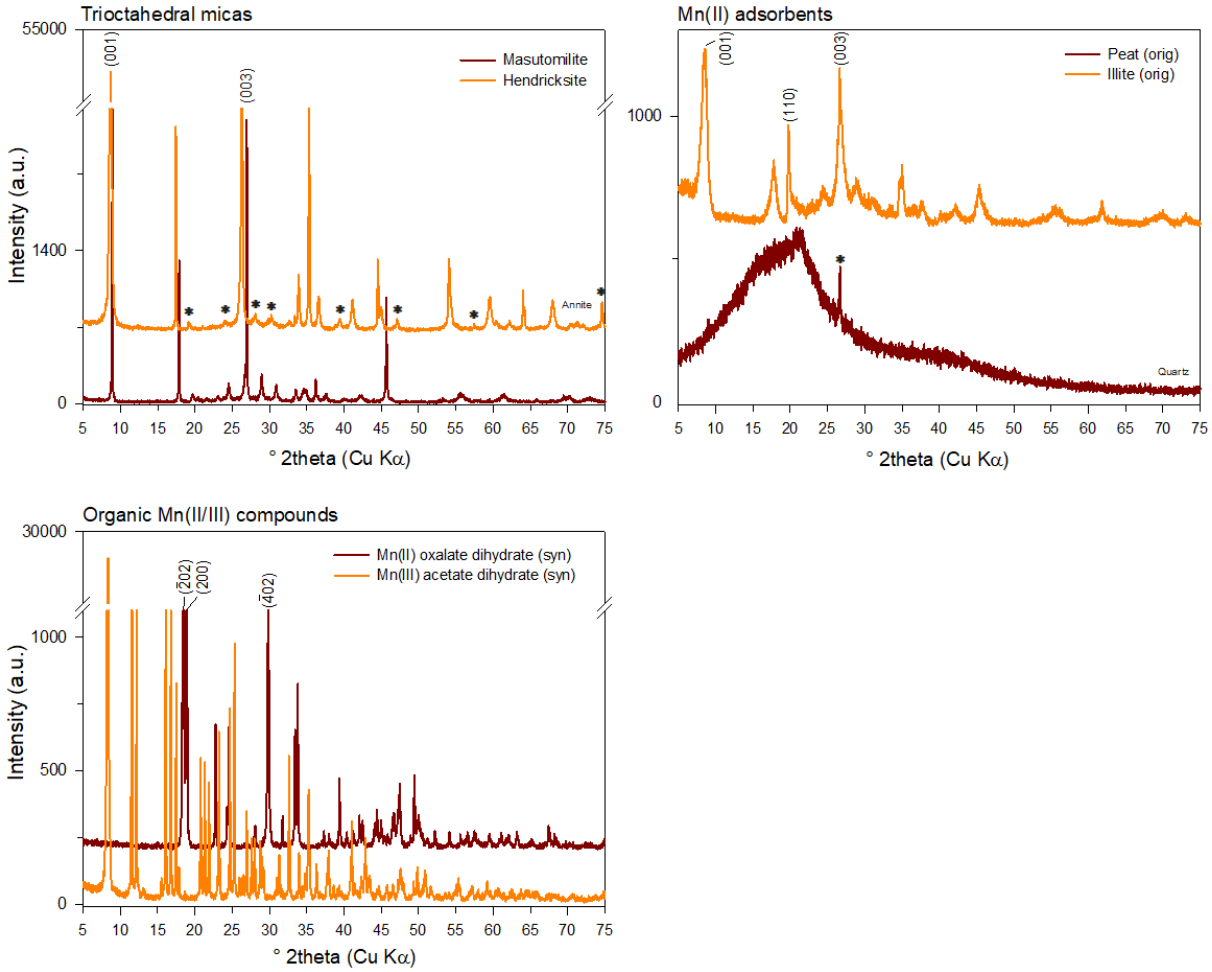

Figure S2. Diffractograms of trioctahedral micas, the Mn(II) adsorbents illite and peat, and organic Mn(II)/(III) compounds. Main reflections are indexed and asterisks indicate impurities (see text for further details).

Table S1. Crystallographic properties and literature references or powder diffraction file (pdf) numbers used for the evaluation of XRD patterns of Mn reference compounds

Mineral	Crystal system	Space group	Literature reference or reference pattern (pdf no.)
Phyllomanganates			
Acid Na-birnessite (hex, syn)	Hexagonal	-	Villalobos et al. (2003)
δ-MnO_2	Hexagonal	-	Villalobos et al. (2003)
Na-birnessite (tricl, syn)	Triclinic	-	Villalobos et al. (2003)
Tectomanganates			
Cryptomelane	Monoclinic	*I*2/*m*	Cryptomelane (00-044-1386)
Cryptomelane (syn)	Monoclinic	*I*2/*m*	Cryptomelane (00-044-1386)
Pyrolusite	Tetragonal	$P4_2/mnm$	Pyrolusite syn (01-081-2261)
			Manganite (01-088-0649)
Pyrolusite (syn)	Tetragonal	$P4_2/mnm$	Pyrolusite syn (01-081-2261)
Ramsdellite	Orthorhombic	*Pbnm*	Ramsdellite (00-043-1455)
Romanèchite (Ba-free)	Monoclinic	C2/m	Romanèchite (00-014-0627)
Todorokite (nat)	Monoclinic	*P*2/*m*	Todorokite (00-038-0475)
Oxide minerals without layer or tunnel structure			
Bixbyite (nat)	Cubic	*Ia*3	Bixbyite C (01-075-0894)
Bixbyite (syn)	Cubic	*Ia*3	Bixbyite C (01-075-0894)
Hausmannite	Tetragonal	$I4_1/amd$	Hausmannite calc. (01-080-0382)
Manganosite (syn)	Cubic	*Fm*3*m*	Manganosite (01-075-1090)
Mn(III) oxyhydroxides			
Manganite (syn)	Monoclinic	$P2_1/c$	Manganite (00-088-0649)
Groutite	Orthorhombic	*Pnma*	Groutite (01-088-0648)
			Calcite (00-005-0586)
			Manganite (01-088-0649)
Carbonate, phosphate, and silicate minerals			
Braunite	Tetragonal	$I4_1/acd$	Braunite-1Q (v00-033-0904)
			Quartz (01-079-1910)
Hendricksite	Monoclinic	*B2/m*	Hendricksite-1M (00-019-0544)
			Annite-1 (00-045-1444)
Masutomilite	Monoclinic	*C2*	Masutomilite (00-029-0822)
Rhodochrosite	Trigonal	$R\bar{3}c$	Rhodochrosite, syn (00-044-1472)
Triplite	Monoclinic	*I*2/*a*	Triplite (00-005-0621)
			Zwiselite (00-021-0811)
Organic Mn(II/III) compounds			
Mn(II) oxalate dihydrate (syn)	Monoclinic	*C*2/*c*	Mn oxalate dihydrate (00-025-0544)
Mn(III) acetate dihydrate (syn)	-	-	-
Adsorbed Mn(II) species			
Illite	Monoclinic	*C*2/*m*	Illite-1 (00-029-1496)
			Montmorillonite (00-029-1499)
			Illite-Montmorillonite (00-035-0652)
Peat	-	-	Quartz (01-083-0539)

3. Chemical characterization of Mn reference compounds

Based on chemical compositions determined by EPMA and acid digestions followed by ICP-OES measurements, empirical mineral formulas were calculated after normalization to oxygen (Table 1). Fractional amounts of Mn^{2+}, Mn^{3+}, and Mn^{4+} per formula unit were determined by charge-balance calculations (Deer, 1992). All chemical analysis results are summarized in Table S2. Detection limits for each element measured are provided in Table S3. For acid digestions, ~100 mg of powdered sample material was placed in Teflon beakers with screw caps. Acid reagents used were 69% HNO_3 (suprapur, Roth), 37% HCl (p.a., Roth), and, if necessary, 40% HF (p.a., Merck) and 30% H_2O_2 (suprapur, Merck). The peat material was previously combusted at 550 °C overnight in a ceramic crucible and quantitatively transferred to a Teflon beaker. The illite sample was previously digested in 3 mL HNO_3 and 5 mL HF overnight at 120 °C. Afterwards, the peat and illite samples were treated identically to all other samples. Sample powders of all compounds were digested at 120-140 °C in aqua regia (3:1 (v/v) HCl:HNO_3) for 12-24 hours. After complete dissolution and vaporization of reagents, the samples were finally taken up in 3% (w/w) HNO_3 and elemental concentrations in solutions determined by ICP-OES (Agilent 5900 SVDV). All samples were digested at least in duplicate. Data quality was monitored by including procedural and measurements blanks. The accuracy of digestions was determined by comparing measured element concentrations of USGS BHVO-1 (basalt) and NIST SRM 2710a (Montana I Soil) reference materials with their certified values. Percent recoveries were always >96%.

Notes on empirical formula calculations. The determination of correct empirical mineral formulas for birnessite modifications is complex. Especially the calculation of vacancies is closely related to the valence of structural Mn cations (Drits et al., 1997; Villalobos et al., 2003). For example, Drits et al. (1997) showed that different empirical mineral formulas ($Na_{0.6}Mn^{4+}_{1.4}$-$Mn^{3+}_{0.6}O_4$ and $Na_{0.6}Mn^{4+}_{1.85}vac_{0.15}O_4$; vac = lattice vacancy) can be calculated from the same chemical birnessite analysis. Variable proportions of each Mn valence might be present in members of the birnessite family, and there is also the possibility of O atom replacements by OH groups and the formation of layer vacancies (Drits et al., 1997). Villalobos et al. (2006) stated the mineral formula of hexagonal acid Na-birnessite with $H_{0.06}K_{0.18}(H_2O)_{0.54}Mn^{3+}_{0.08}(H_2O)_{0.24}$-$[Mn^{4+}_{0.88},vac_{0.12}]O_2$, and we adopted this formula since the mineral synthesis was exactly carried out as described in this study. The same is true for triclinic Na-birnessite and δ-MnO_2, whose formulas were given by Villalobos et al. (2003) as $Na_{0.26}(Mn^{4+}_{0.74}$-$Mn^{3+}_{0.26})O_2$ and $Na_{0.24}(H_2O)_{0.72}(Mn^{4+}_{0.94},vac_{0.06})O_2$, respectively. Formula calculation of natural and synthetic cryptomelane was based on 16 O atoms and 9 cations. As for hollandite, Mn in cryptomelane is mainly reported as Mn^{4+} and Mn^{3+} (Biagioni et al., 2013; Post et al., 1982). Similar to these studies, we also used the assumption of Mn^{4+} and Mn^{3+} prevalence in cryptomelanes. For Ba-free romanèchite, the mineral formula calculation based on 24 O atoms (Shen et al., 2004) did not provide results consistent with elemental analysis. Therefore, the formula calculation was based on oxygen and cation numbers typical for Ba-romanèchite, that is, 6 cations, 10 O atoms, and one H_2O molecule as given in Anthony et al. (2003).

Table S2. Average compositions of Mn reference compounds determined by EPMA and acid digestions (ICP-OES). Chemical data were recalculated into atoms per formula unit (apfu) based on the number of oxygens given below. Numbers in parentheses represent standard deviations of the last significant figure.

	Acid Na-birnessite (hex, syn)	**Bixbyite**	**Braunite**	**Cryptomelane (nat)**	**Cryptomelane (syn)**	**δ-MnO_2**
wt.%	**ICP-OES** *N* **= 3**[a]	**EPMA** *N* **= 4**	**EPMA** *N* **= 6**	**EPMA** *N* **= 3**	**ICP-OES** *N* **= 1**	**ICP-OES** *N* **= 2**
P_2O_5	n.d.[b]	b.d.l.[c]	b.d.l.	b.d.l.	n.d.	n.d.
SiO_2	0.00(0)	b.d.l.	9.26(80)	0.37(0)	0.01	0.00(0)
TiO_2	n.d.	0.15(2)	b.d.l.	b.d.l.	n.d.	n.d.
Al_2O_3	b.d.l.	1.44(7)	0.07(10)	0.42(4)	0.01	b.d.l.
Cr_2O_3	0.01(0)	b.d.l.	b.d.l.	b.d.l.	0.01	0.00(0)
Fe_2O_3	b.d.l.	10.41(27)	b.d.l.	b.d.l.	0.00	b.d.l.
MnO	70.27(47)	77.37(46)	79.02(120)	73.91(37)	79.87	62.78(15)
BaO	0.00	b.d.l.	b.d.l.	0.09(0)	b.d.l.	b.d.l.
CaO	b.d.l.	b.d.l.	1.38(26)	0.30(1)	0.03	b.d.l.
FeO	n.a.[d]	n.a.	n.a.	n.a.	n.a.	n.a.
MgO	0.00	b.d.l.	b.d.l.	b.d.l.	0.00	0.00(0)
PbO[e]	0.37(4)	n.d.	n.d.	n.d.	0.36	0.14(14)
SrO	n.d.	b.d.l.	b.d.l.	0.21(2)	n.d.	n.d.
ZnO	0.00(0)	b.d.l.	b.d.l.	0.30(1)	0.00	0.00(0)
K_2O	5.49(29)	b.d.l.	b.d.l.	4.84(10)	5.81	b.d.l.
Li_2O[e]	0.30(42)	n.d.	n.d.	n.d.	b.d.l.	b.d.l.
Na_2O	b.d.l.	b.d.l.	b.d.l.	0.25(2)	b.d.l.	6.09(125)
Cl	n.d.	b.d.l.	b.d.l.	b.d.l.	n.d.	n.d.
F	n.d.	b.d.l.	b.d.l.	b.d.l.	n.d.	n.d.
Total	**76.44**	**89.37(23)**	**89.73(71)**	**80.68(51)**	**86.10**	**69.01(129)**
O = Cl, F						
H_2O calculated[f]						
CO_2 calculated[f]						
Total corrected	**n.d.**	**98.10(27)**	**97.74(77)**	**96.07(63)**	**102.66**	**n.d.**
apfu based on:						
Moles O[g]		3.00	12.00	16.00	16.00	
Moles cations		2.00	8.00	9.00	9.00	
Moles H_2O						
Moles OH						
apfu						
P^{5+}		b.d.l.	b.d.l.	b.d.l.	0.00	
Mn^{4+}		0.00(0)	0.00(0)	6.73(3)	6.79	
Si^{4+}		b.d.l.	0.95(8)	0.05	0.00	
Ti^{4+}		0.00(0)	b.d.l.	b.d.l.	0.00	
Al^{3+}		0.05(0)	0.01(1)	0.06(1)	0.00	
Cr^{3+}		b.d.l.	b.d.l.	b.d.l.	0.00	
Fe^{3+}		0.21(1)	b.d.l.	b.d.l.	0.00	
Mn^{3+}		1.74(1)	6.08(16)	1.22(5)	1.31	
Ba^{2+}		b.d.l.	b.d.l.	0.00(0)	b.d.l.	
Ca^{2+}		b.d.l.	0.15(3)	0.04(0)	0.00	
Fe^{2+}		0.00(0)	b.d.l.	b.d.l.	0.00	
Mg^{2+}		b.d.l.	b.d.l.	b.d.l.	0.00	
Mn^{2+}		0.00(0)	0.80(8)	0.00(0)	0.00	
Pb^{2+}		n.d.	n.d.	n.d.	0.01	
Sr^{2+}		b.d.l.	b.d.l.	0.02(0)	0.00	
Zn^{2+}		b.d.l.	b.d.l.	0.03(0)	0.00	
K^+		b.d.l.	b.d.l.	0.78(1)	0.89	
Li^+		n.d.	n.d.	n.d.	b.d.l.	
Na^+		b.d.l.	b.d.l.	0.06(0)	b.d.l.	
H^+		-	-	-	-	
Cl		b.d.l.	b.d.l.	b.d.l.	-	
F		b.d.l.	b.d.l.	b.d.l.	-	

[a]*N* = number of spots/samples analyzed. [b]n.d. = not determined. [c]b.d.l. = below detection limit (Table S3). [d]n.a. = not applicable. [e]PbO and Li_2O determined from ICP-OES measurements. [f]Calculated from stoichiometry. H_2O for hendricksite and masutomilite calculated 'by difference' such as to yield Σ(OH, F) = 2.0 and for triplite Σ(O, OH, F) = 1.0. [g]Moles (O, OH, F) for hendricksite, masutomilite, and triplite.

Table S2. (continued)

	Groutite	Hausmannite	Hendricksite	Manganite (syn)	Masutomilite	Na-birnessite (tricl, syn)
wt.%	**EPMA** *N* = 4	**EPMA** *N* = 3	**EPMA** *N* = 3	**ICP-OES** *N* = 1	**EPMA** *N* = 4	**ICP-OES** *N* = 2
P_2O_5	b.d.l.	b.d.l.	b.d.l.	n.d.	b.d.l.	n.d.
SiO_2	0.22(10)	b.d.l.	33.94(3)	0.01	51.09(47)	0.00(0)
TiO_2	b.d.l.	b.d.l.	0.21(1)	n.d.	b.d.l.	n.d.
Al_2O_3	0.25(7)	b.d.l.	11.86(4)	0.01	22.74(43)	0.02(2)
Cr_2O_3	b.d.l.	b.d.l.	b.d.l.	0.01	b.d.l.	0.00(0)
Fe_2O_3	b.d.l.	0.77(56)	-	0.01	-	0.00(0)
MnO	77.77(70)	90.92(79)	10.69(14)	84.80	3.15(24)	71.14(25)
BaO	0.57(82)	b.d.l.	0.23(2)	b.d.l.	b.d.l.	0.00(0)
CaO	b.d.l.	0.00(0)	b.d.l.	0.01	b.d.l.	0.01(0)
FeO	-	-	3.99(6)	-	b.d.l.	
MgO	0.35(5)	0.04(2)	6.09(2)	b.d.l.	b.d.l.	0.00(0)
PbO[e]	n.d.	n.d.	n.d.	0.38	b.d.l.	0.40(5)
SrO	b.d.l.	b.d.l.	b.d.l.	n.d.	b.d.l.	n.d.
ZnO	b.d.l.	b.d.l.	20.72(9)	0.00	0.08(2)	b.d.l.
K_2O	b.d.l.	b.d.l.	8.73(17)	b.d.l.	9.96(22)	0.01(1)
Li_2O[e]	n.d.	n.d.	n.d.	b.d.l.	5.68(0)	b.d.l.
Na_2O	b.d.l.	b.d.l.	0.41(0)	b.d.l.	0.32(8)	8.42(47)
Cl	b.d.l.	b.d.l.	b.d.l.	n.d.	0.08(2)	n.d.
F	b.d.l.	b.d.l.	b.d.l.	n.d.	9.70(48)	n.d.
Total	79.16(36)	91.73(32)	96.85(26)	85.22	102.80(111)	80.01(28)
O = Cl, F			0.00(0)		4.10(20)	
H_2O calculated[f]	10.25(6)		3.55(0)	10.22		
CO_2 calculated[f]						
Total corrected	**98.17(32)**	**98.55(37)**	**100.41(27)**	**105.00**	**98.70(96)**	**n.d.**
apfu based on:						
Moles O[g]	1.50	4.00	12.00	1.50	12.00	
Moles cations	1.00	3.00	8.00	1.00	8.00	
Moles H_2O			1.00			
Moles OH	1.00			1.00		
apfu						
P^{5+}	b.d.l.	b.d.l.	b.d.l.	0.00	b.d.l.	
Mn^{4+}	0.00(0)	0.00(0)	0.00(0)	0.00	0.00(0)	
Si^{4+}	0.00(0)	b.d.l.	2.83(0)	0.00	3.43(3)	
Ti^{4+}	b.d.l.	b.d.l.	0.01(0)	0.00	b.d.l.	
Al^{3+}	0.00(0)	b.d.l.	1.17(0)	0.00	1.80(1)	
Cr^{3+}	b.d.l.	b.d.l.	b.d.l.	0.00	b.d.l.	
Fe^{3+}	b.d.l.	0.02(2)	0.00(0)	0.00	b.d.l.	
Mn^{3+}	0.98(1)	1.98(2)	0.00(0)	1.00	0.00(0)	
Ba^{2+}	0.00(0)	b.d.l.	0.01(0)	b.d.l.	b.d.l.	
Ca^{2+}	b.d.l.	0.00(0)	b.d.l.	0.00	b.d.l.	
Fe^{2+}	b.d.l.	0.00(0)	0.28(0)	0.00	b.d.l.	
Mg^{2+}	0.01(0)	0.00(0)	0.76(0)	b.d.l.	b.d.l.	
Mn^{2+}	0.00(0)	1.00(0)	0.76(1)	0.00	0.18(1)	
Pb^{2+}	n.d.	n.d.	n.d.	0.00	n.d.	
Sr^{2+}	b.d.l.	b.d.l.	b.d.l.	0.00	b.d.l.	
Zn^{2+}	b.d.l.	b.d.l.	1.28(1)	0.00	0.00(0)	
K^+	b.d.l.	b.d.l.	0.93(2)	b.d.l.	0.85(1)	
Li^+	n.d.	n.d.	0.00(0)	b.d.l.	1.53(2)	
Na^+	b.d.l.	b.d.l.	0.07(0)	b.d.l.	0.04(1)	
H^+	1.00(0)	-	1.98(0)	1.00	0.00(0)	
Cl^-	b.d.l.	b.d.l.	b.d.l.	n.d.	0.01(0)	
F^-	b.d.l.	b.d.l.	b.d.l.	n.d.	2.06(9)	

[a]*N* = number of spots/samples analyzed. [b]n.d. = not determined. [c]b.d.l. = below detection limit (Table S3). [d]n.a. = not applicable. [e]PbO and Li_2O determined from ICP-OES measurements. [f]Calculated from stoichiometry. H_2O for hendricksite and masutomilite calculated 'by difference' such as to yield Σ(OH, F) = 2.0 and for triplite Σ(O, OH, F) = 1.0. [g]Moles (O, OH, F) for hendricksite, masutomilite, and triplite.

Table S2. (continued)

	Pyrolusite	Ramsdellite	Rhodochrosite	Romanèchite (Ba-free, syn)	Todorokite	Triplite
wt.%	**EPMA** ***N*** **= 5**	**EPMA** ***N*** **= 4**	**EPMA** ***N*** **= 3**	**ICP-OES** ***N*** **= 2**	**EPMA** ***N*** **= 4**	**EPMA** ***N*** **= 3**
P_2O_5	b.d.l.	b.d.l.	b.d.l.	b.d.l.	b.d.l.	31.45(2)
SiO_2	0.13(7)	0.17(10)	b.d.l.	b.d.l.	0.17(4)	b.d.l.
TiO_2	b.d.l.	b.d.l.	b.d.l.	0.00(0)	b.d.l.	0.16(0)
Al_2O_3	0.84(18)	0.37(34)	b.d.l.	b.d.l.	b.d.l.	b.d.l.
Cr_2O_3	b.d.l.	b.d.l.	b.d.l.	b.d.l.	b.d.l.	b.d.l.
Fe_2O_3	b.d.l.	b.d.l.	0.44(62)	b.d.l.	b.d.l.	-
MnO	79.33(26)	79.55(45)	55.39(148)	77.16(91)	67.00(42)	34.94(14)
BaO	0.20(4)	0.07(4)	b.d.l.	b.d.l.	0.67(18)	b.d.l.
CaO	0.06(1)	0.21(6)	0.79(21)	b.d.l.	1.94(11)	2.46(1)
FeO	-	-	-	-	-	23.86(16)
MgO	b.d.l.	0.07(4)	0.21(2)	b.d.l.	1.48(26)	0.93(4)
PbO[e]	n.d.	n.d.	n.d.	0.38(3)	n.d.	n.d.
SrO	b.d.l.	b.d.l.	b.d.l.	b.d.l.	2.36(55)	b.d.l.
ZnO	b.d.l.	b.d.l.	1.88(21)	0.00(0)	1.09(5)	0.11(1)
K_2O	b.d.l.	b.d.l.	b.d.l.	b.d.l.	0.82(9)	b.d.l.
Li_2O[e]	n.d.	n.d.	n.d.	b.d.l.	n.d.	n.d.
Na_2O	b.d.l.	0.05(1)	0.08(1)	7.42(3)	1.08(12)	b.d.l.
Cl^-	b.d.l.	b.d.l.	b.d.l.	b.d.l.	b.d.l.	b.d.l.
F^-	b.d.l.	b.d.l.	b.d.l.	b.d.l.	b.d.l.	6.68(9)
Total	**80.57(28)**	**80.48(23)**	**58.79(98)**	**85.07(94)**	**76.62(83)**	**100.60(0)**
O = Cl, F						2.81(4)
H_2O calculated[f]				3.81	8.73(5)	0.85(0)
CO_2 calculated[f]			38.34(7)			
Total corrected	**98.46(33)**	**98.42(24)**	**97.08(91)**	**104.46(109)**	**98.42(88)**	**99.99(4)**
apfu based on:						
Moles O[g]	2.00	2.00	1.00	10.00	12.00	5.00
Moles cations	1.00	1.00	1.00	6.00	7.00	3.00
Moles H_2O				1.00	3.00	
Moles OH						
apfu						
P^{5+}	b.d.l.	b.d.l.	b.d.l.	b.d.l.	b.d.l.	0.99(0)
Mn^{4+}	0.99(0)	0.99(1)	0.00(0)	4.16(2)	5.15(1)	0.00(0)
Si^{4+}	0.00(0)	0.00(0)	b.d.l.	b.d.l.	0.02(0)	b.d.l.
Ti^{4+}	b.d.l.	b.d.l.	b.d.l.	0.00(0)	b.d.l.	0.00(0)
Al^{3+}	0.01	0.01(1)	b.d.l.	b.d.l.	b.d.l.	b.d.l.
Cr^{3+}	b.d.l.	b.d.l.	b.d.l.	b.d.l.	b.d.l.	b.d.l.
Fe^{3+}	b.d.l.	b.d.l.	0.00(1)	b.d.l.	b.d.l.	0.00(0)
Mn^{3+}	0.00(0)	0.00(0)	0.00(0)	0.75(2)	0.00(0)	0.00(0)
Ba^{2+}	0.00(0)	0.00(0)	b.d.l.	b.d.l.	0.03(1)	b.d.l.
Ca^{2+}	b.d.l.	0.00(0)	0.02(0)	b.d.l.	0.22(1)	0.10(0)
Fe^{2+}	b.d.l.	b.d.l.	0.00(0)	0.00(0)	b.d.l.	0.75(1)
Mg^{2+}	b.d.l.	0.00(0)	0.01(0)	b.d.l.	0.23(4)	0.05(0)
Mn^{2+}	0.00(0)	0.00(0)	0.94(1)	0.00(0)	0.80(3)	1.11(0)
Pb^{2+}	n.d.	n.d.	n.d.	0.01(0)	n.d.	n.d.
Sr^{2+}	b.d.l.	b.d.l.	b.d.l.	b.d.l.	0.14(3)	b.d.l.
Zn^{2+}	b.d.l.	b.d.l.	0.03(0)	0.00(0)	0.08(0)	0.00(0)
K^+	b.d.l.	b.d.l.	b.d.l.	b.d.l.	0.11(1)	b.d.l.
Li^+	n.d.	n.d.	n.d.	b.d.l.	n.d.	n.d.
Na^+	b.d.l.	0.00(0)	0.00(0)	1.08(1)	0.22(2)	b.d.l.
H^+	-	-	-	2.00(0)	-	0.21(0)
Cl^-	b.d.l.	b.d.l.	b.d.l.	b.d.l.	b.d.l.	b.d.l.
F^-	b.d.l.	b.d.l.	b.d.l.	b.d.l.	b.d.l.	0.79(1)

[a]*N* = number of spots/samples analyzed. [b]n.d. = not determined. [c]b.d.l. = below detection limit (Table S3). [d]n.a. = not applicable. [e]PbO and Li_2O determined from ICP-OES measurements. [f]Calculated from stoichiometry. H_2O for hendricksite and masutomilite calculated 'by difference' such as to yield Σ(OH, F) = 2.0 and for triplite Σ(O, OH, F) = 1.0. [g]Moles (O, OH, F) for hendricksite, masutomilite, and triplite.

Table S3. Detection limits (µg/g) of EPMA and ICP-OES analysis

Element	EPMA	ICP-OES
Al	318	0.061
Ba	308	0.004
Ca	259	0.145
Cl	69	n.d.
Cr	334	0.182
F	1,318	n.d.
Fe	338	0.018
K	572	1.583
Li	n.d.	0.018
Mg	234	0.184
Mn	825	0.026
Na	210	0.324
P	564	n.d.
Pb	n.d.	0.047
Si	392	0.211
Sr	555	n.d.
Ti	273	n.d.
Zn	439	0.055

n.d. = not determined.

4. Manganese K-edge XAS of Mn reference compounds

Sample preparation. Samples were hand-ground to a very fine powder in an agate mortar. For transmission measurements (absorber concentration: >20 g/kg), powders were diluted with boron nitride and CEREOX® wax (Fluxana) such as to yield an edge-step absorption, µx, of ~1 and prepared as pressed pellets (Ø: 1.3 cm) sealed with Kapton® tape. Samples for fluorescence measurements were directly filled into sample holders and sealed with Kapton® tape (BL 7-3 (SSRL), P64 and 65 (DESY)). At beamline 5-BM-D (APS), pellets for transmission-mode measurements were mounted into a Lincam cell.

Manganese K-edge EXAFS fits. Figures S3 and S4 show k^3-weighted Mn K-edge EXAFS spectra, their Fourier-transform magnitudes and real parts as well as corresponding model fits (dotted lines) of all Mn reference compounds. Table S4 lists literature sources used to compare interatomic distances extracted from shell-fit analyses and summarized in Figure 7.

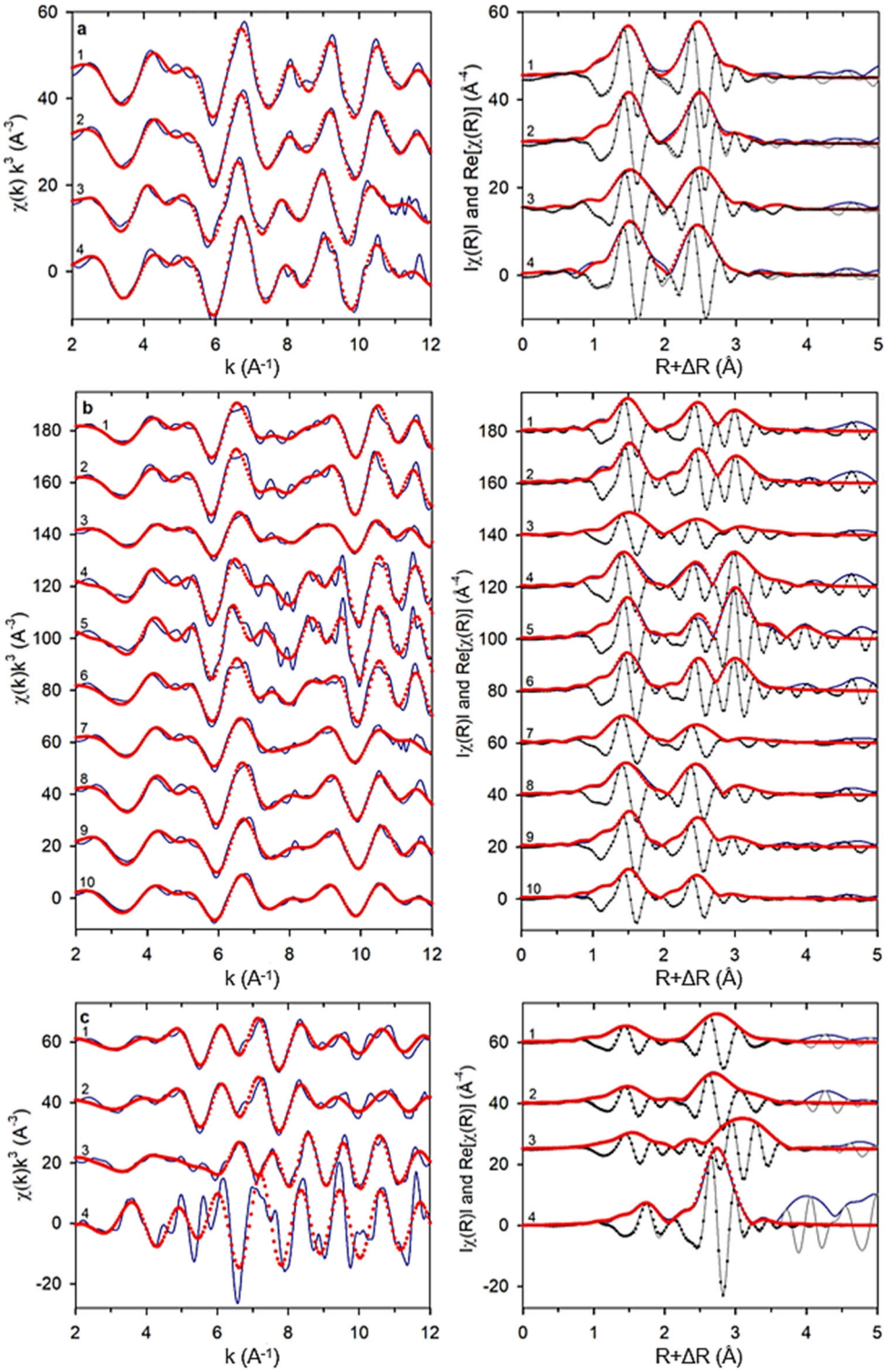

Figure S3. Phyllomanganates (a): 1 - acid Na-birnessite (hex, syn), 2 - δ-MnO_2 (syn), 3 - lithiophorite, 4 - Na-birnessite (tricl, syn); **Tectomanganates (b):** 1 - cryptomelane (nat), 2 - cryptomelane (syn), 3 – hollandite s.s., 4 - pyrolusite, 5 - pyrolusite (syn), 6 - ramsdellite, 7 - romanèchite (nat), 8 - romanèchite (Ba-free, syn), 9 - todorokite, 10 - todorokite (syn); **Oxide minerals without layer or tunnel structure (c):** 1 - bixbyite (nat), 2 - bixbyite (syn), 3 - hausmannite, 4 - manganosite (syn).

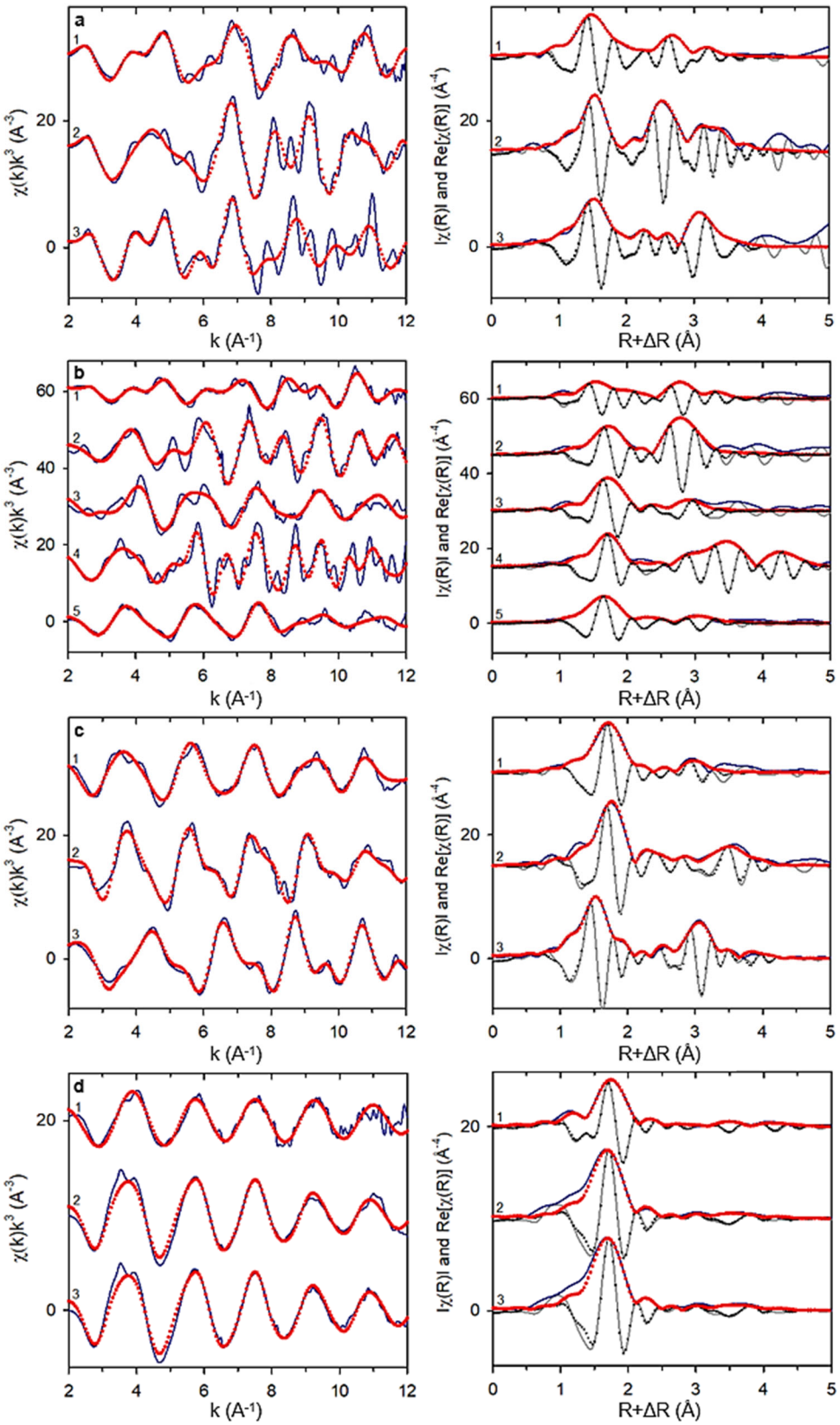

Figure S4. Mn(III) oxyhydroxides (a): 1 - feitknechtite (syn), 2 - groutite, 3 - manganite (syn); **Carbonate, phosphate, and silicate minerals (b):** 1 - braunite, 2 - hendricksite, 3 - masutomilite, 4 - rhodochrosite, 5 - triplite; **Organic Mn(II/III) compounds (c):** 1 - Mn(II) acetate tetrahydrate, 2 - Mn(II) oxalate dihydrate, 3 - Mn(III) acetate dihydrate; **Adsorbed Mn(II) species (d):** 1 - Mn(II) ads. illite pH7, 2 - Mn(II) ads. peat pH5, 3 - Mn(II) ads. peat pH7.

Table S4. Literature references used to compare interatomic distances (Fig. 7)

Reference	Literature reference
Phyllomanganates	
Acid Na-birnessite (hex, syn)	Webb et al. (2005)
	Bargar et al. (2009)
δ-MnO_2 (syn)	Webb et al. (2005)
	Ahmad et al. (2019)
Lithiophorite	McKeown and Post (2001)
	Manceau and Combes (1988)
Na-birnessite (tricl, syn)	Bargar et al. (2009)
	Webb et al. (2005)
	McKeown and Post (2001)
Tectomanganates	
Hollandite	McKeown and Post (2001)
	Manceau and Combes (1988)
Pyrolusite	Silvester et al. (1997)
	McKeown and Post 2001
	Manceau and Combes (1988)
	Elzinga and Kustka (2015)
Ramsdellite	Silvester et al. (1997)
	McKeown and Post (2001)
	Manceau and Combes (1988)
Romanèchite	Silvester et al. (1997)
	McKeown and Post (2001)
Todorokite (syn)	Webb et al. (2005)
Todorokite	McKeown and Post (2001)
	Manceau and Combes (1988)
Oxide minerals without layer or tunnel structure	
Bixbyite (syn)	Longo et al. (2010)
Bixbyite (nat)	Ahmad et al. (2019)
Hausmannite	Longo et al. (2010)
Manganosite (syn)	Ressler et al. (1999)
Mn(III) oxyhydroxides	
Manganite (syn)	Mackle et al. (1993)
Groutite	Scheinost et al. (2001)
Feitknechtite	Ressler et al. (1999)
	Mackle et al. (1993)
Carbonate, phosphate, and silicate minerals	
Rhodochrosite	Lee et al. (2002)
	Effenberger et al. (1981) (XRD)

5. Statistical XANES comparisons

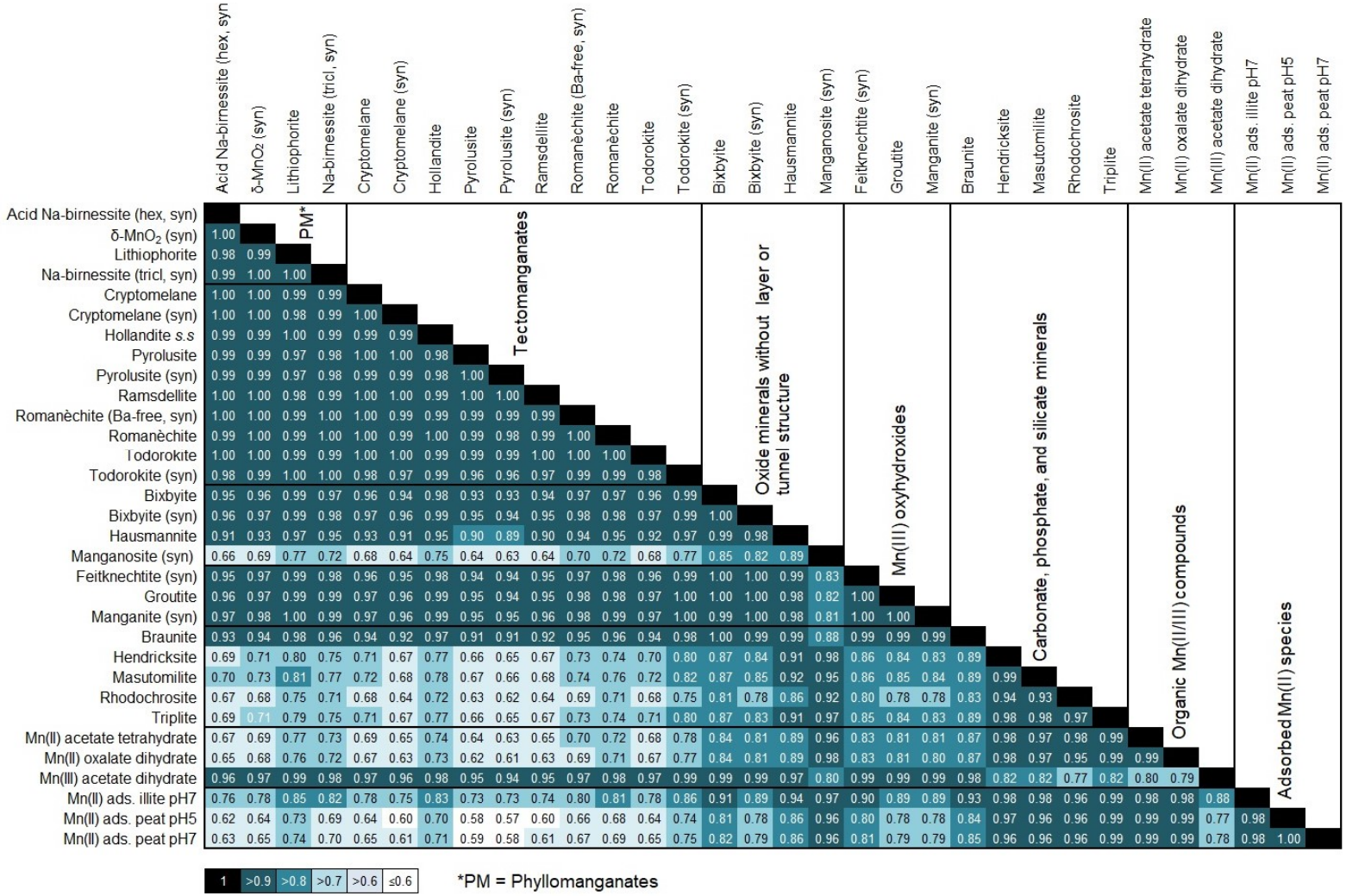

Figure S5. Pearson correlation matrix for normalized XANES spectra (6,530-6,600 eV) of Mn reference compounds. Only significant correlations (p <0.05) are listed.

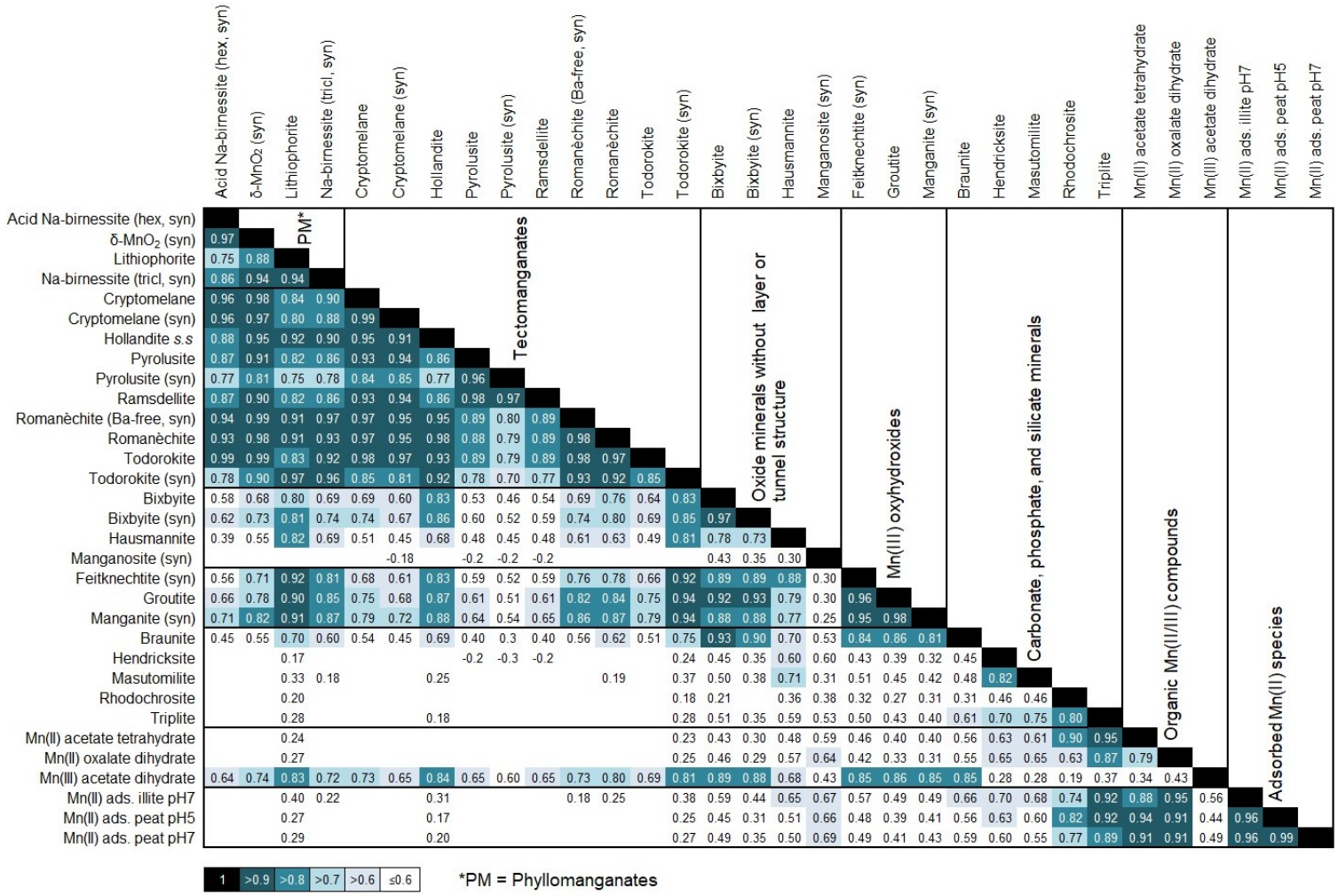

Figure S6. Pearson correlation matrix for first-derivative XANES spectra (6,530-6,600 eV) of Mn reference compounds. Only significant correlations (p <0.05) are listed.

6. PCA output parameters for Mn K-edge EXAFS spectra

Table S5. Output parameters for the first ten PCs obtained from PCA analysis of k^2-weighted EXAFS spectra (k = 2.0-11.5 Å^{-1}, E_0 = 6,563 eV) of Mn reference compounds

Component	Eigenvalue	Total variance	Cumulative eigenvalue	Cumulative variance
1	17.94	56.08	17.94	56.08
2	4.26	13.33	22.21	69.40
3	3.45	10.80	25.66	80.20
4	1.56	4.87	27.22	85.06
5	1.14	3.56	28.36	88.62
6	0.86	2.70	29.22	91.32
7	0.62	1.95	29.84	93.26
8	0.47	1.47	30.32	94.74
9	0.41	1.28	30.73	96.02
10	0.27	0.83	30.99	96.85

7. References

Ahmad, A., van der Wal, A., Bhattacharya, P. and van Genuchten, C.M. (2019) Characteristics of Fe and Mn bearing precipitates generated by Fe(II) and Mn(II) co-oxidation with O_2, MnO_4 and HOCl in the presence of groundwater ions. Water Research 161, 505-516.

Anthony, J.W., Bideaux, R.A., Bladh, K.W., and Nichols, M.C. (2003) Handbook of Mineralogy. Mineralogical Society of America, Chantilly, VA 20151-1110, USA. http://www.handbookofmineralogy.org/.

Bargar, J.R., Fuller, C.C., Marcus, M.A., Brearley, A.J., De la Rosa, M.P., Webb, S.M. and Caldwell, W.A. (2009) Structural characterization of terrestrial microbial Mn oxides from Pinal Creek, AZ. Geochimica et Cosmochimica Acta 73, 889-910.

Biagioni, C., Capalbo, C. and Pasero, M. (2013) Nomenclature tunings in the hollandite supergroup. European Journal of Mineralogy 25, 85-90.

Chukhrov, F.V., Drits, V.A., Gorshkov, A.I., Sakharov, B.A. and Dikov, Y.P. (1987) Structural models of vernadite. International Geology Review 29, 1337-1347.

Chukhrov, F.V. and Gorshkov, A.I. (1980) Reply to R. Giovanoli's comment. Mineralium Deposita 15, 255-257.

da Silva, A.L., de Oliveira, A.H., and Fernandes M.L.S. (2011) Influence of preferred orientation of minerals in the mineralogical identification process by X-ray diffraction, Proceedings of the International Nuclear Atlantic Conference (INAC), Belo Horizonte, MG, Brazil, 24–28 October 2011.

Deer, W.A., Robert A.H., and Zussman J. (1992) An Introduction to the Rock-Forming Minerals, 2nd ed. Longman, 712, London.

Dohrmann, R., Rüping, K.B., Kleber, M., Ufer, K. and Jahn, R. (2009) Variation of preferred orientation in oriented clay mounts as a result of sample preparation and composition. Clays and Clay Minerals 57, 686-694.

Drits, V.A., Silvester, E., Gorshkov, A.I. and Manceau, A. (1997) Structure of synthetic monoclinic Na-rich birnessite and hexagonal birnessite: I. Results from X-ray diffraction and selected-area electron diffraction. American Mineralogist 82, 946-961.

Effenberger, H., Mereiter, K. and Zemann, J. (1981) Crystal structure refinements of magnesite, calcite, rhodochrosite, siderite, smithonite, and dolomite, with discussion of some aspects of the stereochemistry of calcite type carbonates. Zeitschrift für Kristallographie-Crystalline Materials 156, 233-243.

Elzinga, E.J. and Kustka, A.B. (2015) A Mn-54 radiotracer study of Mn isotope solid–liquid exchange during reductive transformation of vernadite (δ-MnO_2) by aqueous Mn(II). Environmental Science & Technology 49, 4310-4316.

Grangeon, S., Lanson, B., Lanson, M. and Manceau, A. (2008) Crystal structure of Ni-sorbed synthetic vernadite: a powder X-ray diffraction study. Mineralogical Magazine 72, 1279-1291.

Hoffmann, M., Mikutta, C. and Kretzschmar, R. (2012) Bisulfide reaction with natural organic matter enhances arsenite sorption: Insights from X-ray absorption spectroscopy. Environmental Science & Technology 46, 11788-11797.

Lee, Y.J., Reeder, R.J., Wenskus, R.W. and Elzinga, E.J. (2002) Structural relaxation in the $MnCO_3$-$CaCO_3$ solid solution: a Mn K-edge EXAFS study. Physics and Chemistry of Minerals 29, 585-594.

Longo, A., Liotta, L.F., Carlo, G.D., Giannici, F., Venezia, A.M. and Martorana, A. (2010) Structure and the metal support interaction of the Au/Mn oxide catalysts. Chemistry of Materials 22, 3952-3960.

Mackle, P., Charnock, J.M., Garner, C.D., Meldrum, F.C. and Mann, S. (1993) Characterization of the manganese core of reconstituted ferritin by X-ray absorption spectroscopy. Journal of the American Chemical Society 115, 8471-8472.

Manceau, A. and Combes, J.M. (1988) Structure of Mn and Fe oxides and oxyhydroxides: A topological approach by EXAFS. Physics and Chemistry of Minerals 15, 283-295.

McKeown, D.A. and Post, J.E. (2001) Characterization of manganese oxide mineralogy in rock varnish and dendrites using X-ray absorption spectroscopy. American Mineralogist 86, 701-713.

Post, J.E. (1999) Manganese oxide minerals: Crystal structures and economic and environmental significance. Proceedings of the National Academy of Sciences 96, 3447-3454.

Post, J.E., Von Dreele, R.B. and Buseck, P.R. (1982) Symmetry and cation displacements in hollandites: Structure refinements of hollandite, cryptomelane and priderite. Acta Crystallographica Section B: Structural Crystallography and Crystal Chemistry 38, 1056-1065.

Ressler, T., Brock, S.L., Wong, J. and Suib, S.L. (1999) Multiple-scattering EXAFS analysis of tetraalkylammonium manganese oxide colloids. The Journal of Physical Chemistry B 103, 6407-6420.

Scheinost, A.C., Stanjek, H., Schulze, D.G., Gasser, U. and Sparks, D.L. (2001) Structural environment and oxidation state of Mn in goethite-groutite solid-solutions. American Mineralogist 86, 139-146.

Shen, X., Ding, Y., Liu, J., Laubernds, K., Zerger, R.P., Polverejan, M., Son, Y.-C., Aindow, M. and Suib, S.L. (2004) Synthesis, characterization, and catalytic applications of manganese oxide octahedral molecular sieve (OMS) nanowires with a 2×3 tunnel structure. Chemistry of Materials 16, 5327-5335.

Shen, X.F., Ding, Y.S., Liu, J., Cai, J., Laubernds, K., Zerger, R.P., Vasiliev, A., Aindow, M. and Suib, S.L. (2005) Control of Nanometer-Scale Tunnel Sizes of Porous Manganese Oxide Octahedral Molecular Sieve Nanomaterials. Advanced Materials 17, 805-809.

Silvester, E., Manceau, A. and Drits, V.A. (1997) Structure of synthetic monoclinic Na-rich birnessite and hexagonal birnessite: II. Results from chemical studies and EXAFS spectroscopy. American Mineralogist 82, 962-978.

Turner, S. and Post, J.E. (1988) Refinement of the substructure and superstructure of romanechite. American Mineralogist 73, 1155-1161.

Villalobos, M., Lanson, B., Manceau, A., Toner, B. and Sposito, G. (2006) Structural model for the biogenic Mn oxide produced by *Pseudomonas putida*. American Mineralogist 91, 489-502.

Villalobos, M., Toner, B., Bargar, J. and Sposito, G. (2003) Characterization of the manganese oxide produced by *Pseudomonas putida* strain MnB1. Geochimica et Cosmochimica Acta 67, 2649-2662.

Webb, S.M., Tebo, B.M. and Bargar, J.R. (2005) Structural characterization of biogenic Mn oxides produced in seawater by the marine *Bacillus sp.* strain SG-1. American Mineralogist 90, 1342-1357.